Arabian Journal of Chemistry (2022) **15**, 103983

King Saud University

Arabian Journal of Chemistry

www.ksu.edu.sa
www.sciencedirect.com

ORIGINAL ARTICLE

Silica-coated magnetic palladium nanocatalyst for Suzuki-Miyaura cross-coupling

Md. Lutfor Rahman [a], Mohd Sani Sarjadi [a], Mohammed Salim Akhter [b], John J. Hannan [c], Shaheen M. Sarkar [c]

[a] *Faculty of Science and Natural Resources, Universiti Malaysia Sabah, Kota Kinabalu 88400, Sabah, Malaysia*
[b] *Department of Chemistry, University of Bahrain, Bahrain*
[c] *Department of Applied Sciences, Technological University of the Shannon: Midlands Midwest, Moylish, Limerick V94, EC5T, Ireland*

Received 13 January 2022; accepted 17 May 2022
Available online 23 May 2022

KEYWORDS

Aryl halide;
Organoboronic acid;
Schiff base;
Magnetic nanoparticles;
Palladium catalyst

Abstract A silica-coated magnetically separable Schiff-base palladium nanocatalyst was developed. Amorphous silica was used to encapsulate the magnetic Fe_3O_4 and an organic amine functionality was added to the silica surface. The amino group was treated with 1, 10-phenanthroline-2,9-dicarboxaldehyde to produce a Schiff-base, which was then treated with palladium to produce the silica coated magnetic Schiff-base palladium nanocatalyst. The palladium nanocatalyst was fully characterized using several spectroscopic techniques. The HR-SEM image of silica coated Fe_3O_4 revealed a globular shape with a diameter of 145 nm, along with this the average palladium nanoparticle size was 3.5 ± 0.6 nm. The successful functionalization and the appearances of the palladium species as a magnetic catalyst was confirmed by FT-IR and XRD analysis. The palladium nanocatalyst was successfully applied for the construction of C—C bonds via Suzuki-Miyaura reaction. With a variety of organoboronic acids, the catalyst displayed great performance for electron-poor and electron-rich aryl halides, resulting in excellent yields of the corresponding cross-coupling products. The magnetic catalyst was retrieved from the reaction vial using an external strong magnet, and it was reused seven times without a significant drop in the production of the corresponding biaryl product.

1. Introduction

Over the last few decades, environmentally friendly chemistry based on metal catalysts has prompted interest in the fields of cosmetics, materials science, medicines, biotechnology, pesticides, advanced chemistry, and agrochemicals that reduce fuel consumption and pollution (Li et al., 2020; He et al., 2020; Rohani et al., 2019; Baran and Nasrollahzadeh, 2019). Heck (Mastalir et al., 2020), Hiyama (Karami et al., 2018), Sonogashira (Campisciano et al., 2019), Negishi

E-mail addresses: lotfor@ums.edu.my (Md. Lutfor Rahman), shaheen.sarkar@tus.ie (S.M. Sarkar)
Peer review under responsibility of King Saud University.

ELSEVIER Production and hosting by Elsevier

https://doi.org/10.1016/j.arabjc.2022.103983

(Gonzalez-Perez et al., 2012), Stille (Nikoorazm et al., 2018), and Suzuki cross-coupling reaction (Takale et al., 2019) are amongst the most common applications of metal catalysts, particularly palladium. Among these cross-coupling reactions, Suzuki coupling, which involves coupling an aryl halide with an aryl boronic acid in the presence of a metal salt such as $Pd(OAc)_2$, $Pd(PPh_3)_4$, or $Pd(dtbpf)Cl_2$, has gained a lot of attention because of its extensive use in the industrial synthesis of biaryl products (Mehta et al., 2020; Mutoh et al., 2020; Delaney et al., 2020; Espinoza et al., 2019). Palladium salts are commonly employed in the cross-coupling reactions, a drawback of these are their significant costs and potential challenges associated with their use including the need for organic solvents, inert gases, catalytic sensitivities, large-scale use, purification and recycling, which often make homogeneous catalytic reactions non-economic and environmental unfriendly (Arpad, 2011; Fihri et al., 2011). As a result, to address the inherent disadvantages of homogeneous metal catalysts, homogeneous metal catalysts on a solid support or the creation of innovative heterogeneous catalysts that reduce costs and allow metal species to be recycled are required (Okumura et al., 2015). Manipulation of supporting materials could be a viable technique for generating an environmentally friendly catalyst with improved activity while eliminating the requirement for expensive metal species. In order to improve these heterogeneous catalytic systems, palladium catalysts immobilized on a variety of organic and inorganic substrates have recently been used including magnetic Pd@IO-Chitosan (Shaikh and Pamidimukkala, 2021), silica (Qiu et al., 2008; Sarkar et al., 2015), Fe_3O_4@SiO_2-NMIM-Pd (Dong et al., 2021), Fe_3O_4 (Nasrollahzadeh et al., 2020), microbeads (Baran and Nasrollahzadeh, 2020), Schiff base palladium (Neshat et al., 2021), polymers (Yamada et al., 2012; Sultana et al., 2016), cellulose (Li et al., 2019) kaolin/$NiFe_2O_4$ (Çalıskan and Baran, 2021), carbon materials (Xi et al., 2018), carbon nitride (Alam and Sarkar, 2011), MOF (Sarkar et al., 2015; Wang et al., 2019); bis-NHC palladium pincer complex (Rajabi et al., 2021); *coleus amboinicus* supported PdNPs@CA (Bathula et al., 2020) and covalent organic frameworks (Fan et al., 2019; Ma et al., 2017). These exhibit superior environmental friendly, sustainable and reusable potential. It is a major challenge to design efficient green heterogeneous catalysts that are facile to synthesise, can be applied in the aqueous phase, be stable at higher reaction temperatures and have reduced metal leaching challenges from their support systems or agglomeration resulting in low activity in long-term service (Sakina et al., 2021). However, there is an inconsistency between the size and isolation of non-dimensional carriers. Due to the larger specific surface area, the use of nanomaterials could result in larger metal anchoring sites and lower steric hindrance than with larger supports. Nonetheless, due to the small size of the nanocatalyst, conventional separation methods make it difficult to separate the nanocatalyst from the reaction system. To maximize metal catalyst availability while preventing metal species leaching, a true heterogeneous catalyst must be developed by attaching metal species uniformly throughout the solid support. The support material with the appropriate chelating groups can influence catalytic reactivity by controlling the electronic structure of the active sites via interfacial interactions, in addition to contributing to uniform diffusion and stability of the active metal species (Yang et al., 2018; Chen et al., 2018). Magnetic nanoparticles (MNPs) have gained popularity in recent years due to their large surface area and unique properties, which have led to particular and potential applications in many fields like energy storage (Li et al., 2018), magnetic resonance imaging (MRI) (Meng et al., 2020; Wei et al., 2020), gene delivery (Amani et al., 2021), hyper-thermal agents (Lu et al., 2021), drug delivery (Taherian et al., 2021), cell sorting (Moradi et al., 2021), and catalysis (Ye et al., 2021; Wang et al., 2021; Tamoradi et al., 2020). The use of MNPs as catalysts is primarily based on the presence of strong magnetic moments and the ease of product / catalyst separation by an external magnet, as well as their high stability and chemical durability, recyclability, and benign classification in the context of sustainable chemistry (Nasrollahzadeh, 2018; Tukhani et al., 2018; Paula et al., 2020). These ideal characteristics reduce the need for time-consuming and labour intensive separation

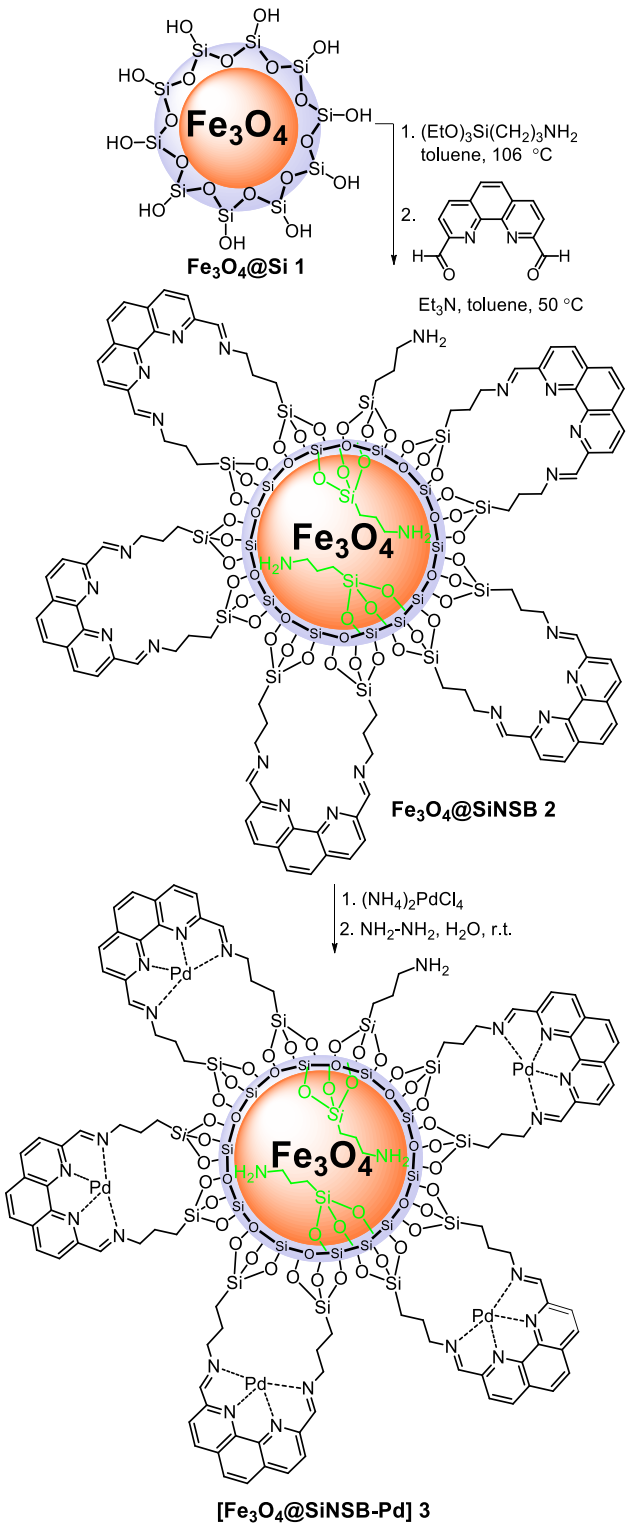

Scheme 1 Synthesis of silica coated magnetic **[Fe_3O_4@SiNSB-Pd] 3**.

methods while maintaining catalytic activity and allowing for continuous catalysis. However, uncoated magnetic nanoparticles tend to clump together, resulting in a reduction of surface area, accelerated biodegradation during the catalytic cycle (Nosrati et al., 2019), which result in a drop in catalytic activity. Magnetic nanoparticles can be prevented from aggregating by covering them with carbonized materials

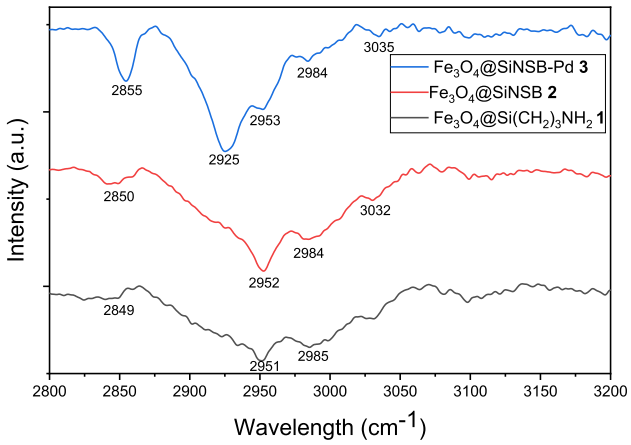

Fig. 1 FT-IR images of synthesized materials.

(Wei et al., 2021), polymers (You et al., 2021), or metal oxides (Elhampour and Nemati, 2017). This offers greater protection under mild acidic conditions, is unreactive in aqueous systems, and has a number of beneficial properties, such as large pore volume, large surface area, covalent adherence through various desirable functional groups (Hollingsworth et al., 2016), excellent biocompatibility, adjustable pore size and inhibitory activity. Silicon dioxide was chosen as the best coating material to overcome the drawbacks of pure magnetic nanoparticles (Sun et al., 2016; Maleki et al., 2020; Esmaeilpour et al., 2015). In this research we successfully synthesized a silica-coated magnetic Schiff base palladium nanocatalyst [**Fe_3O_4@SiNSB-Pd**] **3** and utilized it for the construction of C—C bonds through Suzuki-Miyaura cross-coupling reaction. The Suzuki-Miyaura reaction of activated electron-poor and inactivated electron-rich aryl halides with a series of organoboronic acids proceeded facilely with this **Fe_3O_4@SiNSB-Pd** nanocatalyst, yielding biaryl products with excellent yield. The palladium nanocatalyst **Fe_3O_4@SiNSB-Pd** was stable and could be recovered from the reaction vessel using an external magnet. It could also be used seven times without decreasing the production of biaryls substantially.

2. Experimental

2.1. Preparation of magnetic Schiff base [Fe_3O_4@SiNSB] 2

The preparation of Fe_3O_4, **[Fe_3O_4@Si] 1**, followed by amine functionalization of **1** were carried out according to the literature report (Ghasemzadeh and Basir, 2015; Shao et al., 2012; Fekri and Zeinali, 2020). The amine functionalized Schiff-base **[Fe_3O_4@SiNSB] 2** was prepared by the treatment of 1.0 g of **1** with 250 mg of 1,10-phenanthroline-2,9-dicarboxalde hyde (Coogan et al., 2015) in 60 mL of toluene at 80 °C

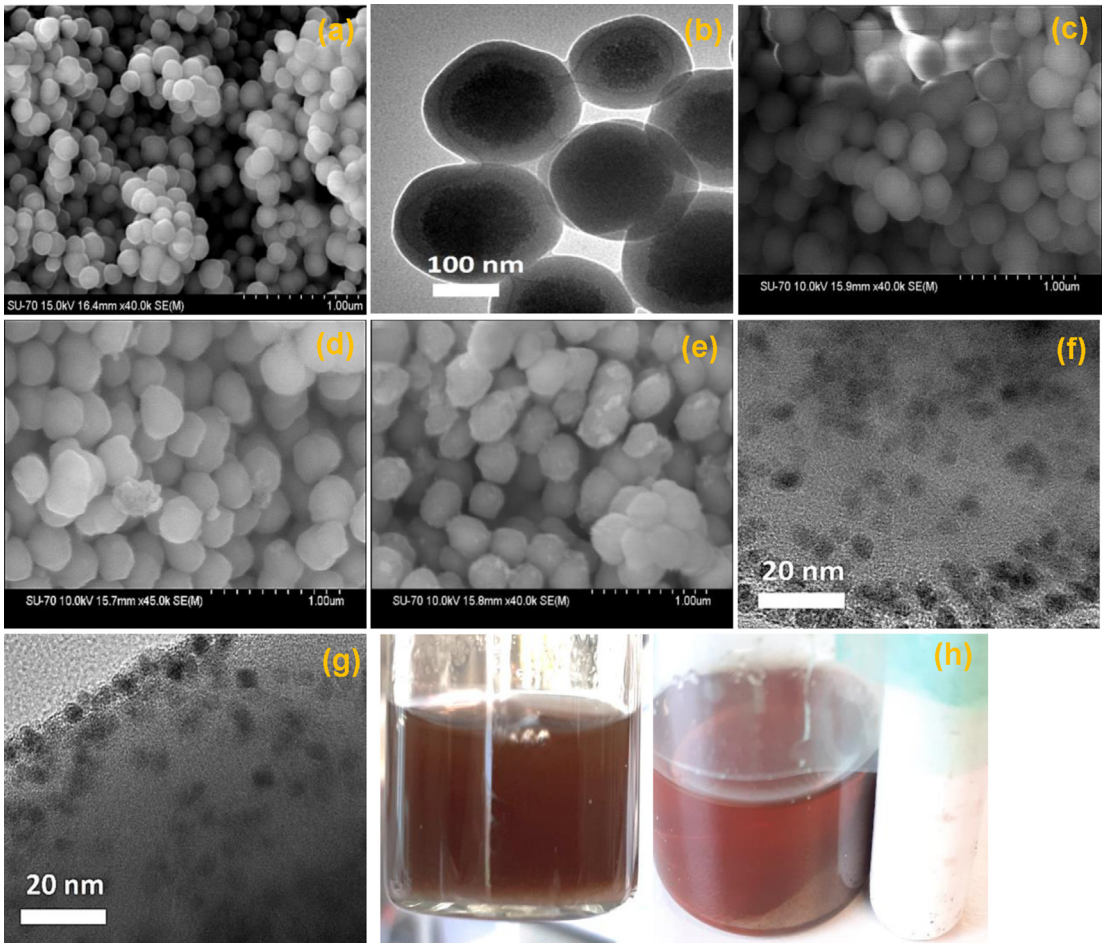

Fig. 2 (a & b) SEM images of **1**, (c) SEM image of **1** after incorporation of amine functionality, (d) SEM image of **2**, (e) SEM image of 3, (f) TEM image of fresh **3**, (g) TEM image of 3rd reused of **3**, (h) recovery of **3**.

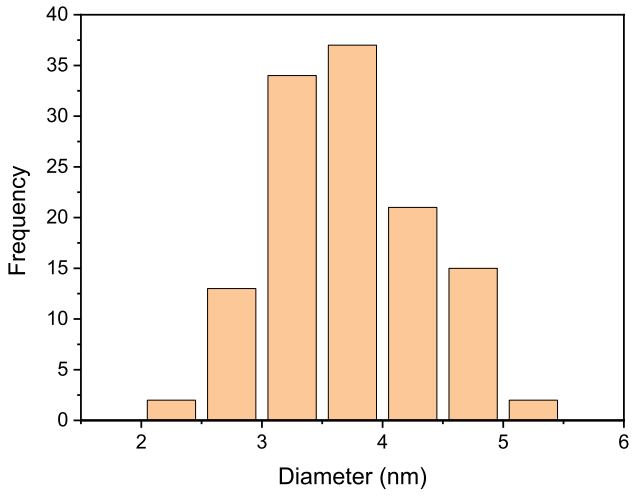

Fig. 3 Palladium nanoparticles size distribution of **3**.

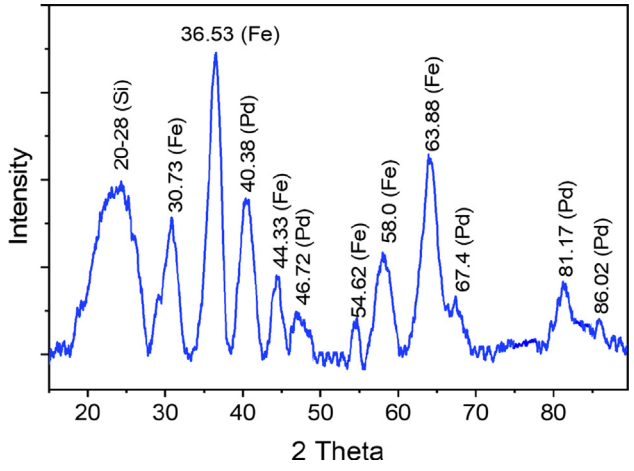

Fig. 4 XRD spectrum of 3.

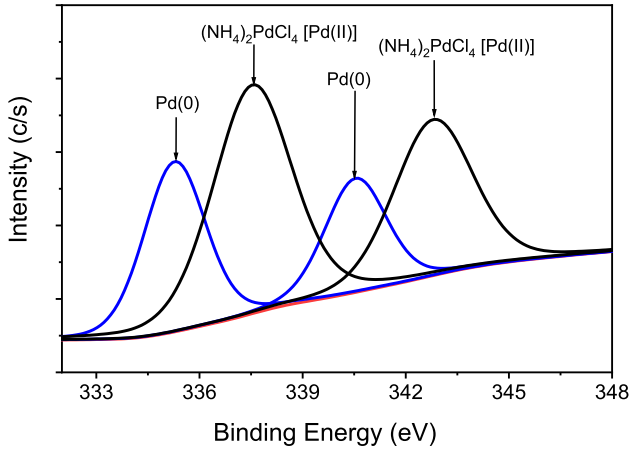

Fig. 5 XPS image of Pd(0) in 3.

overnight. After allowing the reaction mixture to cool to room temperature, the Schiff-base magnetic **2** was filtered, washed with ethanol, and dried at 60 °C for 5 h.

2.2. Preparation of [Fe_3O_4@SiNSB-Pd] 3

An aqueous solution of $(NH_4)_2PdCl_4$ (300 mg, in 25 mL water) was applied dropwise to the synthesized [**Fe_3O_4@SiNSB**] **2** (2.0 g) suspended in 55 mL water. After 3 h at room temperature mixing, 0.5 mL hydrazine hydrate was added and the mixture and stirred for another 2 h. The **Fe_3O_4@SiNSB** turned dark brown, and the resulted silica coated magnetic palladium nanocatalyst **3** was collected by filtration and the solid material was washed with an aqueous solution of methanol and dried for 4 h at 60 °C. ICP-AES study revealed that 0.017 mmol/g of palladium bound with **3**, and TEM investigation revealed that the average nanoparticle size of Pd was 3.5 ± 0.6 nm.

2.3. General procedure of Suzuki-Miyaura reaction

A 10 mL screw-capped vial containing [**Fe_3O_4@SiNSB-Pd**] **3** (0.017 mol% of Pd), aromatic halide (1 mmol), organoboronic acid (1.20 mmol), 2.5 mol equivalent of K_2CO_3, and a mixture of aqueous ethanol (1:1, 2 mL) was heated to 80 °C. The formation of biaryl was continuously monitored by GC analysis. When no aryl halide peak could be seen in the GC chromatogram, the reaction was allowed to cool down at room temperature and diluted with ethyl acetate and water. The ethyl acetate was separated, dried over anhydrous $MgSO_4$ and evaporated using a rotary evaporator. The resulting crude biaryl product was isolated on a short silica gel column chromatography by using ethyl acetate and hexane as an eluent (1:4) with 86% yield. ^{1}HNMR (500 MHz) of **4j**: δ 7.48 (d, 4H, J = 9.9 Hz), 7.23 (d, 4H, J = 6.65 Hz), ^{13}C NMR δ 138.27, 136.68, 129.42, 126.79, 21.72.

3. Results and discussion

The magnetically enhanced nanocatalyst was developed by the introduction of palladium nanoparticles onto a silica-coated Fe_3O_4 core–shell phenanthroline Schiff-base structure. The synthetic steps are outlined in Scheme 1. Fe_3O_4 was prepared by the co-precipitation of Fe^{2+} and Fe^{3+} in an aqueous ammonium hydroxide solution. After successful synthesis of magnetic Fe_3O_4, it was encapsulated by treatment with tetraethyl orthosilicate (TEOS). The resulting Fe_3O_4@SiO_2 core–shell was then treated with (3-aminopropyl) triethoxysilane (APTES) to afford amine (–NH_2) functionalized magnetic silica. The phenanthroline chelating ligand 1,10-phenanthroline-2,9-dicarboxaldehyde (Coogan et al., 2015) was treated with amine functionalized magnetic silica at 80 °C in toluene to yield the magnetic Schiff base [**Fe_3O_4@SiNSB**] **2**. The brown palladium complex was obtained by treating the magnetically silica-coated Schiff-based **2** with ammonium tetrachloropalladate at room temperature. The palladium nanocatalyst [**Fe_3O_4@SiNSB-Pd**] **3** was then treated with hydrazine hydrate to yield a dark brown powder. According to ICP the palladium level in this nanocatalyst **3** was 0.017 mmol/g.

The synthesized magnetic materials and the structure of the palladium nanocatalyst **3** were studied by using several spectroscopic methods. The FT-IR spectra of amino the functionalized **1** showed absorption peaks at 2849 cm^{-1}, 2951 cm^{-1} and 2985 cm^{-1} due to the aliphatic C-H (sp^3) stretching (Fig. 1). However, after incorporation of the phenanthroline chelating ligand onto **2** the absorption peaks at 2850 cm^{-1},

Table 1 Optimization of Suzuki-Miyaura cross-coupling.[a]

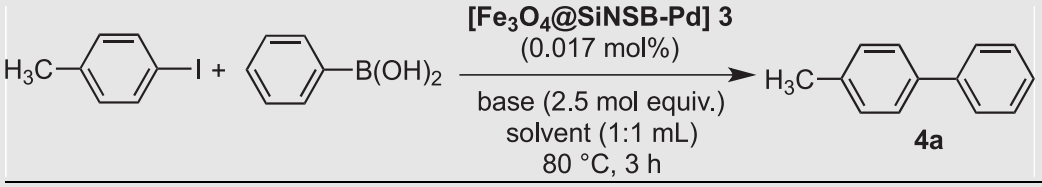

Entry	Base	Solvent	Yield (%)[c]
1	Potassium carbonate	H_2O-EtOH	95
2	Potassium carbonate	H_2O-DMF	90
3	Potassium carbonate	H_2O-THF	74
4	Potassium carbonate	H_2O-DMSO	77
5	Potassium carbonate	H_2O	31
6[b]	Potassium carbonate	H_2O	84
7	Potassium carbonate	H_2O-TBAB	79
8	Potassium phosphate	H_2O-EtOH	89
9	Sodium acetate	H_2O-EtOH	88
10	Sodium carbonate	H_2O-EtOH	89
11	Sodium hydroxide	H_2O-EtOH	78
12	Potassium hydroxide	H_2O-EtOH	79
13[d]	Potassium carbonate	H_2O-EtOH	4

[a] Reaction conditions: 1 mmol of 4-iodotuluene, 1.2 mmol of phenylboronic acid, 2.5 mmol of base, 0.017 mol% of **3**, solvents (1/1 mL), 80 °C for 3 h.
[b] Reaction was carried out at room temperature for 10 h.
[c] Isolated yield.
[d] Reaction was carried out without addition of **3**.

2982 cm^{-1} and 2984 cm^{-1} were observed for aliphatic C-H (sp^3) stretching and additionally 3032 cm^{-1} peak was observed from phenanthroline C-H (sp^2) stretching. Furthermore, after incorporation of palladium, the IR spectrum of **3** shifted to a lower wavenumbers at 2856 cm^{-1}, 2925 cm^{-1} and 2953 cm^{-1} due to the electron transfer from nitrogen atoms to palladium.

The SEM image of the silica encapsulated **Fe_3O_4@SiO_2** core–shell **1** revealed a spherical shape with a diameter of 145 nm (Fig. 2a). The magnified SEM image of **1** (Fig. 2b) clearly show that the Fe_3O_4 nanoparticles were completely encapsulated by silica and that the impregnated Fe_3O_4 nanoparticles were evenly distributed within the silica.

After incorporation of the amino functionality, the SEM image showed a spherical shape with greater diameter than **1** (Fig. 2c). Furthermore, the relatively larger diameter of **2** was also observed due to the incorporation of the organic chelating group with **1** (Fig. 2d). The SEM image of **3** after the introduction of palladium nanoparticles revealed an unsmooth spherical shape (Fig. 2e) due to chelating group aggregations in order to produce the palladium complex. The excellent dispersion of palladium nanoparticles over the silica coated magnetic Fe_3O_4 was revealed by TEM investigation of **3** (Fig. 2f). TEM examination was used to estimate the size of the palladium nanoparticles, and the average particle size distribution is shown in Fig. 3. The average size of palladium nanoparticles was found to be 3.5 ± 0.6 nm on the distribution diagram. Fig. 2g shows the TEM investigation of the 3rd reuse of **3**, which clearly demonstrated that the palladium nanoparticles were not agglomerated under the reaction conditions. The magnetic palladium nanocatalyst could be recovered using an external magnetic, as shown in Fig. 2h.

Fig. 4 shows a typical XRD pattern of magnetically silica-coated Schiff based palladium nanocatalyst **3**. For Fe_3O_4 nanoparticles, the six typical peaks 2θ = 30.73, 36.53, 44.33, 54.62, 58.0, and 63.88 were detected based on particular indices (220), (311), (400), (422), (511), and (440). The crystallinity of the Pd-nanoparticles shows five exclusive reflections in the diffraction pattern at 2θ = 40.38° (111), 46.72° (200), 67.4° (220), 81.17° (311) and 86.02° (222) (Khan et al., 2014). The face-centered cubic (fcc) structure of Pd (JCPDS: 870641, space group: Fm3m (225)) (Shankar et al., 2004) may be indexed by these distinctive reflections. In comparison to the other four, the significant reflection at (111) may suggest a favourable development direction for the nanocrystals. Using Scherrer's equation, the average crystallite size of the Pd-nanoparticles (3.6 nm) was calculated from the half width of the (111) reflection. The amorphous structure of the silicon dioxide layer is shown by the broad peak from 20 to 28 (Safavi et al., 2013).

The oxidation status of palladium species in **3** was determined using X-ray photoelectron spectroscopy (XPS). The narrow scan profile XPS of **3** revealed two signals at 335.32 eV and 340.52 eV, respectively, that may be ascribed to $Pd3d_{5/2}$ and $Pd3d_{3/2}$ in Pd° species respectively (Fig. 5) (Zhang et al., 2017).

Following the characterisation of the silica coated magnetic Schiff-based palladium nanocatalyst **3**, the Suzuki-Miyaura C—C bond formation process was examined, with 4-iodoanisole and phenylboronic acid being chosen as the optimal reactants for the C—C bond formation (Table 1). A constant quantity of 0.017 mol % (10 mg) of [**Fe_3O_4@SiNSB-Pd**] **3** was used to screen the Suzuki-Miyaura C—C

Table 2 Scope of Suzuki-Miyaura cross-coupling.

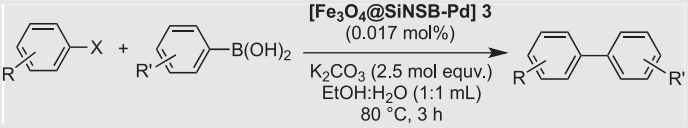

Aryl halide	Boronic acid	Product	Yield (%)
	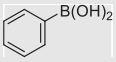	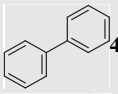 **4b**	X = I, 92 X = Br, 86 X = Cl, 73
	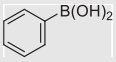	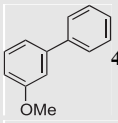 **4c**	X = I, 87 X = Br, 80 X = Cl, 71
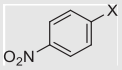	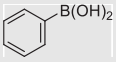	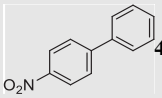 **4d**	X = I, 96 X = Br, 91 X = Cl, 75
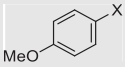	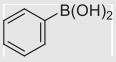	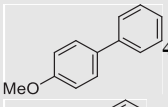 **4e**	X = I, 92 X = Br, 88 X = Cl, 78
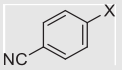	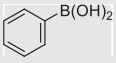	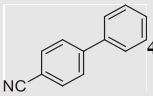 **4f**	X = I, 93 X = Br, 87 X = Cl, 77
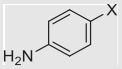	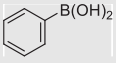	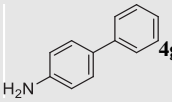 **4g**	X = I, 88 X = Br, 87 X = Cl, 75
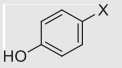	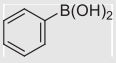	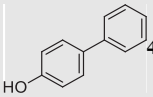 **4h**	X = I, 90 X = Br, 89 X = Cl, 75
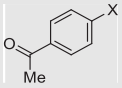	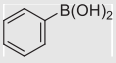	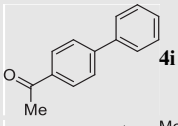 **4i**	X = I, 94 X = Br, 90 X = Cl, 85
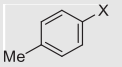	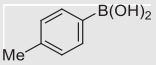	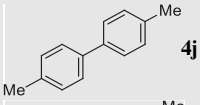 **4j**	X = I, 91 X = Br, 84 X = Cl, 73
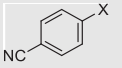	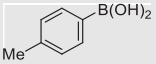	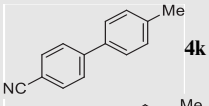 **4k**	X = I, 90 X = Br, 84 X = Cl, 72
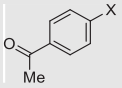	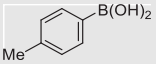	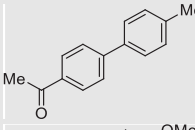 **4l**	X = I, 92 X = Br, 86 X = Cl, 73
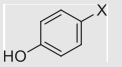	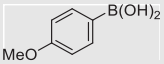	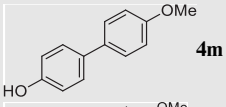 **4m**	X = I, 89 X = Br, 83 X = Cl, 72
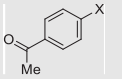	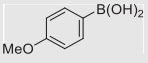	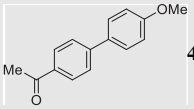 **4n**	X = I, 88 X = Br, 74 X = Cl, 70
		4o	X = I, 90 X = Br, 86 X = Cl, 73
		4p	X = I, 89 X = Br, 78 X = Cl, 70
			X = I, 90

Table 2 (*continued*)

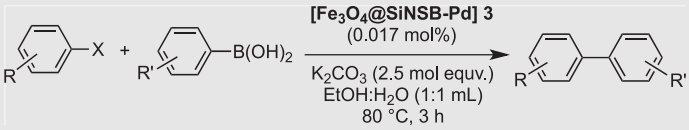

Aryl halide	Boronic acid	Product	Yield (%)
		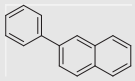 **4q**	X = Br, 85 X = Cl, 74
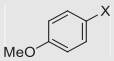	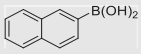	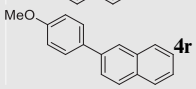 **4r**	X = I, 89 X = Br, 82 X = Cl, 71
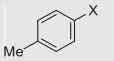	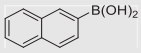	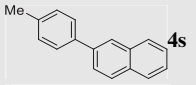 **4s**	X = I, 87 X = Br, 83 X = Cl, 72
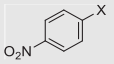	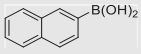	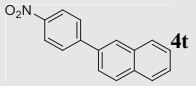 **4t**	X = I, 96 X = Br, 92 X = Cl, 78
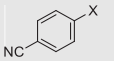	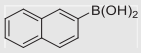	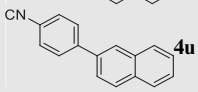 **4u**	X = I, 90 X = Br, 84 X = Cl, 71
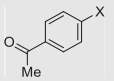	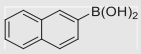	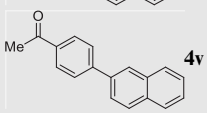 **4v**	X = I, 92 X = Br, 86 X = Cl, 73

[a]Reaction conditions: 1 mmol aryl halide, 1.2 mmol arylboronic acids, 2.5 mmol of K_2CO_3, 0.017 mol% of **3**, H_2O:EtOH (1/1 mL), 80 °C for 3 h.

bond formation reaction. The initial reaction was performed in an aqueous solution of ethanol at 80 °C for 3 h with 4-iodotoluene and phenylboronic acid in the presence of 2.5 mol equivalents of K_2CO_3. The Suzuki-Miyaura reaction was effectively promoted by the magnetic palladium nanocatalyst **3**, yielding the corresponding 4-methyl-1,1′-biphenyl 4a in 95% yield (Table 1, entry 1). When the reactions were carried out using an aqueous solution of *N,N*-dimethylformamide (DMF), tetrahydrofuran (THF) and dimethyl sulfoxide (DMSO), these gave **4a** in 90%, 74% and 77% yield respectively (entries 2-4-) which showed relatively lower yield of **4a** compared to entry 1. Interestingly, when the Suzuki-Miyaura reaction was performed in pure water at 80 °C for 3 h, it gave a 31% yield (entry 5), however 84% yield was obtained when the reaction was continued for 10 h (entry 6).

Furthermore, the addition of a small amount of phase transfer catalyst, such as tetrabutylammonium bromide (TBAB 0.5 mol percent) in pure water, altered the rate of C—C bond formation, yielding **4a** with a 79% yield (entry 7). The formation of **4a** was not improved when the reactions were performed in aqueous ethanol using a variety of bases (entries 8–12). Only 4% yield of **4a** was achieved when the reaction was conducted without adding of **3** (entry 13).

After achieving a satisfactory catalytic performance of **3**, its application in a wide range of substrates were described in Table 2. The magnetic palladium nanocatalyst [**Fe_3O_4@-SiNSB-Pd**] **3** was successfully used in the Suzuki-Miyaura C—C bond formation reaction of activated electron-poor and inactivated electron-rich substituted aryl iodides and phenylboronic acid to yield the respective substituted biaryl products **4b-i** in a range between 87% and 96% yield (Table 2). Since aryl bromide undergoes slower oxidative addition with palladium species, their catalytic reactivity in the cross-coupling reactions showed lower yields than that of aryl iodides. Researchers are interested in using commercially available, inexpensive aryl bromides and chlorides for chemical synthesis, although these aryl halides are known to be poor active sources of aryl in the cross-coupling reactions even at high temperatures. Long reaction times and high catalytic loads were commonly used with commercially available metals/ligands to cope with high temperatures (Zapf et al., 2000). With this in mind, we studied the chemically less reactive aryl bromides and aryl chlorides with aryl boronic acids under the identical reaction conditions in the presence of 0.017 mol percent of **3**. Interestingly, **3** stimulates the cross-coupling reactions of aryl bromides and chlorides with phenylboronic acid, resulting in high yields of the corresponding biaryls **4b-i**. Aryl chlorides showed lower yield of the products compared to aryl iodides and bromides. Similarly, when aryl iodides with electron poor and electron rich groups were combined with substituted phenylboronic acids, the corresponding coupling products **4j-p** were smoothly obtained in up to 92% yield. The less reactive aryl bromides and chlorides were also smoothly promoted in the coupling reactions with substituted phenylboronic acids, yielding the respective products **4j-p** in high yield. The electron poor aryl halides gave higher yields of the respective biaryls than electron rich aryl halides. When using a sterically hindered organoboronic acid, such as 2-naphthylboronic acid, throughout the Suzuki-Miyaura reaction of aryl halides, the cross-coupling reaction proved more

difficult, and the yields of each product were typically poor. With sterically bulky 2-naphthylboronic acid, the magnetic palladium nanocatalyst **3** was effective in forming C—C bonds in all activated and deactivated aryl halides, giving the corresponding biaryls **4q-v** in a range of 71–96% yields.

Dong et al. (2021) recently synthesized *N*-methylimidazole-functionalized Fe_3O_4@SiO_2-NMIM-Pd catalyst, which was employed in the Suzuki-Miyaura cross-coupling reaction to produce biaryls. The cross-coupling reaction was carried out in pure ethanol at 80 °C in the presence of 2 mol% palladium. However, when compared to their report, our catalytic system outperforms it by a factor of a 118. Furthermore, when they performed the cross-coupling reaction with aryl chloride, they found that the formation of biaryl products was poor.

The reusability of heterogeneous catalysts is an essential issue in terms of economic feasibility and sustainability. Therefore, further investigation into the recycling and reuse of **3** (Fig. 6) was carried out. To investigate the reusability of **3** in the C—C bond formation, a separate reaction was carried out according to Table 2, **4d**. The reaction was carried out with 0.13 mol% of **3** in order to make the catalyst easier to handle and separate from the reaction mixture (Eq. (1)). After completion of the first cycle the reaction mixture was allowed to cool to room temperature and diluted with ethyl acetate.

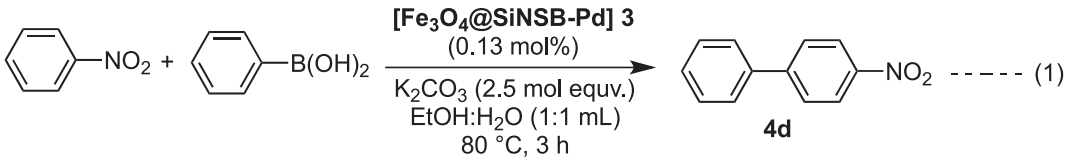

The magnetic palladium nanocatalyst was recovered from the reaction mixture using an external strong magnet (Fig. 2h) and all the liquids were carefully discarded. The solid catalyst was then rinsed with water, methanol and ethyl acetate and dried for 1 h at 60 °C. The reused magnetic palladium nanocatalyst **3** was further used to the next catalytic cycle without changing the reaction parameters. The magnetic catalyst **3** was repeatedly used in up to seven successive runs with high performance without any significant drop of its catalytic activity (Fig. 6). The TEM image (Fig. 2g) of reused **3** confirmed that the magnetic palladium nanoparticles were not aggregated

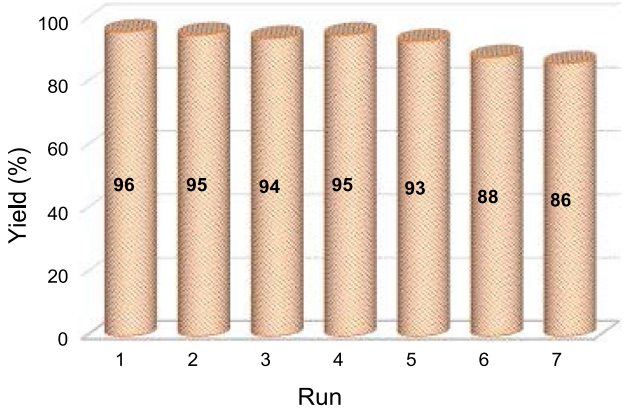

Fig. 6 Recycled experiment using **[Fe_3O_4@SiNSB-Pd] 3**.

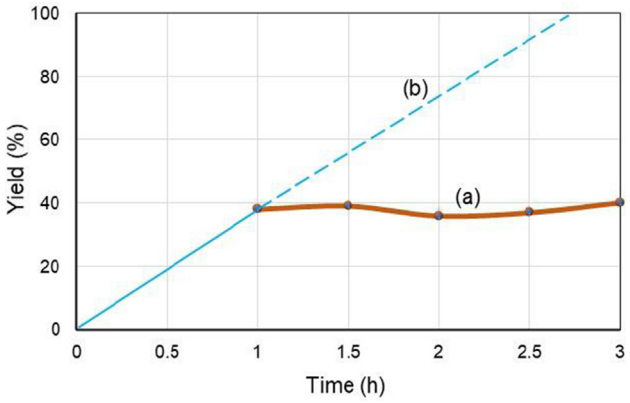

Fig. 7 Heterogeneity of **[Fe_3O_4@SiNSB-Pd] 3**.

under the reaction conditions. We observed that only a slight low yield of the product was formed due to loss of **3** during the catalyst recovery process. Therefore, it was successfully shown that the silica-coated magnetic palladium **3** nanoparticles can be reused with high catalytic performance.

In addition, to assess the heterogeneity of the silica coated magnetic palladium nanocatalyst **3** we also performed a hot filtration experiment (Fig. 7). To verify the heterogeneity of **3** we have carried out two Suzuki-Miyaura reactions of iodobenzene with phenylboronic acid under optimized reaction conditions.

After 1 h of reaction progress, the palladium nanocatalyst **3** was removed (a) using a powerful magnet, and the solution was heated for another 2 h under the same reaction conditions. When the palladium nanocatalyst **3** was removed, the reaction (a) stopped, whereas the controlled reaction (b) progressed smoothly and yielded the desired product with an acceptable yield. As a result, the Suzuki-Miyaura reaction is believed to have occurred in a heterogeneous reaction environment.

4. Conclusion

A silica-coated magnetic Schiff-base palladium nanoparticle was prepared, characterized, and successfully used in the Suzuki-Miyaura cross-coupling reaction to form C—C bonds. The magnetic pallidum nanocatalyst **3** was successfully used in the cross-coupling of activated and deactivated aryl iodides, bromides, and chlorides with a variety of organoboronic acids in aqueous ethanol to produce the corresponding biaryl with high yield. The magnetic catalyst **3** remained stable in the reaction medium, could be completely separated from the reaction mixture, and could be reused seven times without affecting biaryl synthesis.

Author Contributions

This manuscript was prepared by the contributions of all authors. Authors were written, given their valuable comments and approval for the final version of this manuscript.

Declaration of Competing Interest

The authors declare that they have no known competing financial interests or personal relationships that could have appeared to influence the work reported in this paper.

Acknowledgement

The authors are thankful to the Research Management Centre of Universiti Malaysia Sabah, Malaysia and Bernal Institute, University of Limerick, Ireland for support to this work.

Appendix A. Supplementary material

The ^{1}H and ^{13}C NMR spectra for the synthesized biaryl products can be found in the supplementary information section. Supplementary data to this article can be found online at https://doi.org/10.1016/j.arabjc.2022.103983.

References

Alam, M.N., Sarkar, S.M., 2011. React. Kinet. Mech. Catal. 103, 493.
Amani, A., Alizadeh, M.R., Yaghoubi, H., Ebrahimi, H.A., 2021. J. Drug. Deliv. Sci. Tech. 61, 102151.
Arpad, M., 2011. Chem. Rev. 111, 2251–2320.
Baran, T., Nasrollahzadeh, M., 2019. Carbohydr. Polym. 222, 115029.
Baran, T., Nasrollahzadeh, M., 2020. Int. J. Biol. Macromol. 148, 565–573.
Bathula, C., Subalakshmi, K., Ashok Kumar, K., Yadav, H., Ramesh, S., Shinde, S., Shrestha, N.K., Mallikarjuna, K., Kim, H., 2020. Colloides Surf. B 192, 111026.
Çalıskan, M., Baran, T., 2021. Coll. Interfa. Sci. Commun. 43, 100445.
Campisciano, V., Calabrese, C., Liotta, L.F., La Parola, V., Spinella, A., Aprile, C., Gruttadauria, M., Giacalone, F., 2019. Appl. Organomet. Chem. 33, 4848.
Chen, Z.P., Vorobyeva, E., Mitchell, S., Fako, E., Ortuno, M.A., Lopez, N., Collins, S.M., Midgley, P.A., Richard, S., Vile, G., Ramirez, J.P., 2018. Nat. Nanotechnol. 13, 702–707.
Coogan, N.T., Chimes, M.A., Raftery, J., Mocilac, P., Denecke, M.A., 2015. J. Org. Chem. 80, 8684–8693.
Delaney, C.P., Kassel, V.M., Denmark, S.E., 2020. ACS Catal. 10, 73–80.
Dong, Y., Xue, F., Wei, Y., 2021. J. Phy. Chem. Sol. 153, 110007.
Elhampour, A., Nemati, F., 2017. Org. Prep. Proced. Int. 49, 443–458.
Esmaeilpour, M., Javidi, J., Zandi, M., 2015. New J. Chem. 39, 3388–3398.
Espinoza, M.C., Carrillo, J.G.P., Guerra, H.R., Rivera, S.L., Jimenez, F.O., 2019. J. Organomet. Chem. 880, 386–391.
Fan, M., Wang, W.D., Zhu, Y., Sun, X., Zhang, F., Dong, Z., 2019. Appl. Catal. B Environ. 257, 117942.
Fekri, L.Z., Zeinali, S., 2020. Appl. Organometal. Chem., 5629
Fihri, A., Bouhrara, M., Nekoueishahraki, B., Basset, J.M., Polshettiwar, V., 2011. Chem. Soc. Rev. 40, 5181–5203.
Ghasemzadeh, M.A., Basir, M.H.A., Babaei, Masoomeh, 2015. Green Chem. Lett. Rev. 8, 40–49.
Gonzalez-Perez, A.B., Alvarez, R., Faza, O.N., Lera, A.R., Aurrecoechea, J.M., 2012. Organometallics 31, 2053–2058.
He, S., Li, W., Wang, X., Ma, Q., Li, M., Xu, W., Wang, X., Zhao, C., 2020. Appl. Surf. Sci. 506, 144948.
Hollingsworth, J.V., Bhupathiraju, N.V.S.D.K., Sun, J., Lochner, E., Vicente, M.G.H., Russo, P.S., 2016. ACS. Appl. Mater. Inter. 8, 792–801.
Karami, K., Jamshidian, N., Nikazma, M.M., Herves, P., Shahreza, A.R., Karami, A., 2018. Appl. Organomet. Chem. 32, 3978.
Khan, M., Khan, M., Kuniyil, M., Adil, S.F., Warthan, A.A., Alkhathlan, H.Z., Tremel, W., Tahir, M.N., Siddiqui, M.R.H., 2014. Dalton Trans. 43, 9026.
Li, X., Dong, F., Zhang, L., Xu, Q., Zhu, X., Liang, S., Hu, L., Xie, H., 2019. Chem. Eng. J. 372, 516–525.
Li, W., He, S., Xu, W., Wang, X., 2018. Electrochim. Acta 284, 647–654.
Li, W., Wang, X., Li, M., He, S., Ma, Q., Wang, X., 2020. Appl. Catal. B Environ. 268, 118384.
Lu, X., Zhang, Y., Wang, L., Li, G., Gao, J., Wang, Y., 2021. Drug Delivery 28, 380–389.
Ma, H.C., Kan, J.L., Chen, G.J., Chen, C.X., Dong, Y.B., 2017. Chem. Mater. 29, 6518–6524.
Maleki, A., Ledari, R.T., Ghalavand, R., Haji, R.F., 2020. J. Phys. Chem. Solids 136, 109200.
Mastalir, A., Hancsarik, M., Szabo, T., 2020. Appl. Organomet. Chem. 34, 5565.
Mehta, M.M., Boit, T.B., Dander, J.E., Garg, N.K., 2020. Org. Lett. 22, 1–5.
Meng, Z., Li, G., Yiu, S.C., Zhu, N., Leung, C.W., Yu, Z.Q., Manners, I., Wong, W.Y., 2020. Angew. Chem. Int. Ed. 59, 11521–11526.
Moradi, N., Muhammadnejad, S., Delavari, H., Pournoori, N., Oghabian, M.A., Ghafouri, H., 2021. Int. J. Bio. Macromol. 192, 72–81.
Mutoh, Y., Yamamoto, K., Saito, S., 2020. ACS Catal. 10, 352–357.
Nasrollahzadeh, M., 2018. Molecules 23, 2532.
Nasrollahzadeh, M., Bidgoli, N.S.S., Issaabadi, Z., Ghavamifar, Z., Baran, T., Luque, R., 2020. Int. J. Biol. Macromol. 148, 265–275.
Neshat, A., Gholinejad, M., Ozcan, H., Khosravi, F., Mobarakeh, A. M., Zaim, O., 2021. Mol. Cat. 505, 111528.
Nikoorazm, M., Ghorbani, F., Ghorbani-Choghamarani, A., Erfani, Z., 2018. Appl. Organomet. Chem. 32, 4282.
Nosrati, H., Salehiabar, M., Fridoni, M., Abdollahifar, M.A., Manjili, H.K., Davaran, S., Danafar, H., 2019. Sci. Rep. 9, 7173.
Okumura, K., Mushiake, T., Matsui, Y., Ishii, A., 2015. ChemPhysChem 16, 1719–1726.
Paula, A., Devib, M., Sankar Dhar, S., 2020. J. Phys. Chem. Solids 136, 109117.
Qiu, H., Sarkar, S.M., Lee, D.H., Jin, M.J., 2008. Green Chem. 10, 37.
Rajabi, F., Burange, A.S., Voskressensky, L.G., Luque, R., 2021. Molecular Catalysis 515, 111928.
Rohani, S., Ziarati, A., Ziarani, G.M., Badiei, A., Burgi, T., 2019. Catal. Sci. Technol. 9, 3820–3827.
Safavi, A., Banazadeh, A.R., Sedaghati, F., 2013. Anal. Chim. Acta 796, 115.
Sakina, F., Ruiz, C.F., Bedia, J., Sainero, L.G., Baker, R.T., 2021. Catalyst 11, 23.
Sarkar, S.M., Rahman, M.L., Yusoff, M.M., 2015. New J. Chem. 39, 3564–3570.
Sarkar, S.M., Rahman, M.L., Yusoff, M.M., 2015. RSC Adv. 5, 1295.
Shaikh, N., Pamidimukkala, P., 2021. Int. J. Bio. Macromol. 183, 1560–1573.
Shankar, S.S., Rai, A., Ankamwar, B., Singh, A., Ahmad, A., Sastry, M., 2004. Nat. Mater. 3, 482.
Shao, M., Ning, F., Zhao, J., Wei, M., Evans, D.G., Duan, X., 2012. J. Am. Chem. Soc. 134, 1071–1077.
Sultana, T., Mandal, B.H., Rahman, M.L., 2016. S. M. Sarkar 1, 4108.
Sun, W., Yang, W., Xu, Z., Li, Q., Shang, J., 2016. ACS Appl. Mater. Inter. 8, 2035–2047.
Taherian, A., Esfandiari, N., Rouhani, S., 2021. CancerNano. 12, 15.
Takale, B.S., Thakore, R.R., Handa, S., Gallou, F., Reilly, J., Lipshutz, B.H., 2019. Chem. Sci. 10, 8825–8831.
Tamoradi, T., Daraie, M., Heravi, M.M., 2020. Appl. Organomet. Chem. 34, 5538.
Tukhani, M., Panahi, F., Nezhad, A.K., Sustain, A.C.S., 2018. Chem. Eng. 6, 1456–1467.

Wang, G., Lv, K., Chen, T., Chen, Z., Hu, J., 2021. Int. J. Bio. Macromol. 184, 358–368.
Wang, M., Wang, X., Feng, B., Li, Y., Han, X., Lan, Z., Gu, H., Sun, H., Shi, M., Li, H., Li, H., 2019. J. Catal. 378, 153–163.
Wei, Z., Wang, D., Liu, Y., Guo, X., Zhu, Y., Meng, Z., Yu, Z.Q., Wong, W.Y., 2020. J. Mater. Chem. C 8, 10774–10780.
Wei, B., Zhou, C., Yao, Z., Chen, P., Wang, M., Li, Z., Zhou, J., Hou, J., Li, W., 2021. Carbon 184, 232–244.
Xi, J., Sun, H., Wang, D., Zhang, Z., Duan, X., Xiao, J., Xiao, F., Liu, L., Wang, S., 2018. Appl. Catal. B Environ. 225, 291–297.
Yamada, Y.M.A., Sarkar, S.M., Uozumi, Y., 2012. J. Am. Chem. Soc. 134, 3190–3198.
Yang, Y., Reber, A.C., Gilliland, S.E., Castano, C.E., Gupton, B.F., Khanna, S.N., 2018. J. Catal. 360, 20–26.
Ye, L., Liu, X., Lu, Y., 2021. J. Cat. 397, 36–43.
You, J., Wang, L., Zhao, Y., Bao, W., 2021. J. Clean. Prod. 281, 124668.
Zapf, A., Ehrentraut, A., Beller, M., 2000. Angew. Chem. Int. Ed. 39, 4153.
Zhang, H., Yan, X., Huang, Y., Zhang, M., Tang, Y., Sun, D., Xu, L., Wei, S., 2017. Appl. Surf. Sci. 396, 812.